

Supplementary Information

for

Enhanced photothermal absorption in iridescent feathers

Authors: Svana Rogalla^{1*}, Anvay Patil², Ali Dhinojwala², Matthew D. Shawkey¹, Liliana D'Alba¹

¹Evolution and Optics of Nanostructures Group, Department of Biology, University of Ghent, K. L. Ledeganckstraat 35, 9000 Ghent, Belgium

²School of Polymer Science and Polymer Engineering, The University of Akron, Akron, Ohio 44325, United States

*Corresponding Author: srogalla@arcor.de

This Supplementary Information includes

- Supplemental material and methods
- Supplemental figures
- Supplemental tables
- SI References

Supplemental material and methods

Feather area per unit skin surface

Plumage thermal resistance increases linearly with feather area per unit skin surface (pl), thus, pl is inversely related to radiative heat gain [1]. The projected area of feather elements per unit skin surface is the proportion of feather surface which is solid times the number of feather layers overlying the skin. Since we were using museum specimens, we could not measure pl following the procedure by Walsberg et al. [1], which required a destructive procedure to analyze single feathers. Instead, we quantified the feather area per unit skin surface (pl) by counting the numbers of feathers, and averaging length and width of the feathers. To assess the number of feathers, we placed a 5x5 mm² squared plate at skin level beneath the plumage of the analyzed body part until it was no longer visible. We grabbed all feathers above the square with one plier and counted the feathers with the help of a magnifier and another plier (Fig. 3b). For the sake of simplicity, we assumed that the proportion of feather surface which is solid is directly correlated to length and width of the feathers. Thus, we measured length and width of 3 feathers at the spot where we counted the feathers and averaged these values. For the length, we measured the length along the rachis from feather pin to feather tip. For the width we measured the feather's widest part.

Hence, we set the feather area per unit skin surface as:

$$pl = \frac{\text{feather length (mm)} * \text{feather width (mm)} * \text{number of feathers}}{25 \text{ mm}^2}.$$

We are aware that our method might result in an overestimation of the actual pl . However, this simplified and uniform approach can provide an overall idea of the impact of the feather area per unit skin surface (pl) on the heat gain at skin level.

Feather nanostructure

To test how structural composition and distribution of pigments in the integument of sunbird feather barbules affect light and heat absorption, we used optical and heat modeling based on electron microscopy images. To obtain transmission electron microscopy (TEM) images, we embedded barbs and barbules of 6 feathers (non-iridescent white, grey and black; iridescent copper, green and purple) following the protocol described in D'Alba et al. [2] and cut thin (100 - 150 nm) cross sections with a Leica UC-6 ultramicrotome (Leica Microsystems, Germany). Sections were placed on formvar support film copper grids, stained in Uranylless/lead citrate and examined with a JEOL JEM 1010 (Jeol Ltd, Tokyo, Japan) transmission electron microscope. To obtain scanning electron microscopy (SEM) images, we cut thicker sections (5 μm) of the embedded feather barbs and barbules and fixed them with carbon tape on aluminum stubs. Images were taken with a FlexSEM 1000 (Hitachi High-Tech Corporation, Japan) under an accelerating voltage of 5 - 10 kV and working distances ranging from 6.6 to 7.5 mm. We used the TEM and SEM images to assess shape, size and arrangement of the melanosome pigments in the feather barbules. We assessed the length of the melanosomes from the SEM images and averaged height and width measurements of 10 - 15 melanosomes from the TEM images. We further measured the distance between the melanosome layers and assessed the width of the outer keratin layer. Measurements were performed in ImageJ [3].

The white barbule consisted of keratin only, the grey had integrated spherical melanosomes that were arranged randomly, and the black had integrated rods organized in 3 layers at the outer edge of the barbule. In iridescent feather barbules, melanosomes were organized as platelets, whereby the general pattern consisted of an upper layer of keratin, underlying melanin layers followed by a volume of keratin and a mirrored bottom layering. Dimensions and arrangements of melanosomes used to create idealized models of the feather barbules can be found in Figure S2. Barbules were in average 3 μm high, hence we used 3 μm high keratin blocks for the models. To explore if modeled temperatures of feather barbules increase with increasing melanin content, we used a set of models incorporating a melanin layer of different widths ranging from 50 to 2000 nm within a 3 μm block of keratin.

In another set of models, we explored the effect of bulk melanin concentration and distribution within the keratin on optical and thermal properties. Therefore, we used 1.5 μm high keratin blocks, which is half the barbule model, and did not consider the mirrored bottom layering of melanin and keratin. We first tested photothermal properties of melanin concentration by using increasing widths of a single melanin layer (50, 250, 500 and 1000 nm). Since melanosomes in iridescent sunbird feather barbules

were generally arranged in layers, we then tested for the effect of melanin content by increasing the number of 50 nm thick melanin layers (1, 3, 5 and 7 layers). The upper keratin layer was kept 50 nm, an average as assessed from TEM images of the feather barbules.

In a third set of models, we explored the effects of structural arrangement and shape of melanosomes on photothermal properties. Therefore, we used melanosome shapes that are common in feather barbules (spheres, ellipsoids, rods and platelets). For each shape we modeled an organized and a random arrangement of melanin particles within the keratin block. Melanin content within the block was kept constant (ca. 7.3 % of the total system). Particle dimensions are provided in Table S3.

For all models we obtained reflectance, transmittance and absorption profile per wavelength (380 - 2000 nm) using Ansys Lumerical's FDTD solver. We used the detector planar geometry to get average reflectance (light reflected at both specular and diffuse angles). The typical setup of the simulation box is presented in Figure S3. For the refractive indices, we used the Cauchy dispersion in Stavenga et al. [4] with a real part refractive index of 1.554 at 500 nm (imaginary part = 0) for keratin and 1.7428 at 500 nm (imaginary part = 0.0879) for melanin [4]. We calculated the temperatures, attained due to photothermal heating, based on the optical absorption profile as steady state temperature of the material for an ambient temperature of 20°C. Thus, the temperature increase due to photothermal heating was $\Delta T = \frac{q}{h}$, where q is the cumulative energy absorbed based on the product of the absorption of the material and the light intensity per wavelength in W/m^2 and h is the convection coefficient. For the light intensity we used the irradiance of the light bulb (Fig. S1), which was normalized for an intensity of $1000 W/m^2$, the intensity that reached the feather surfaces during experimental heating. For comparison we further modelled temperatures using the solar irradiance spectrum by Gueymard et al. [5]. Modeled temperatures were higher when using the solar spectrum but the trend, which was the variable we were most interested in, remained the same. Thus, for the sake of consistency, all modeled temperatures reported in the manuscript were calculated based on the irradiance of the heat lamp. For the convection coefficient, a variable in fitting the results, we used $10 Wm^{-2}K^{-1}$. We applied the convection coefficient once (on the top side of the keratin block) assuming that we modeled an uppermost feather barbule that lies on the top layer of the feather surface and expected no (or minimal) convection at the bottom.

Statistical analysis

To analyze the effect of feather reflectance on the experimentally measured heat loads on feather surfaces, skin and reference temperatures, we obtained two values describing the response of each sample to the experimental heating: the heating rate k_2 (slope of the linear regression of the heating curve) and the asymptotic maximum temperature T_∞ (average of last 100 seconds of the heating curve). To test whether all heating curves (both at skin level and at the feather surface) reached the asymptote, we first visually inspected the heating curves and then used an augmented Dickey-Fuller test using the R package “tseries” [6]. Both the visual inspection of the heating curves as a function of time and the augmented Dickey-Fuller test confirmed that the time-series of the temperature data is stationary ($p < 0.05$ in $> 99\%$ of 504 heating curves for each surface and skin temperatures), thus that we reach the asymptotic maximum temperature, both at the feather surface and at skin level.

To examine whether the asymptotic maximum temperature of the feather surfaces was influenced by variation in the initial temperature T_0 (mean = $23.58 \pm 0.029^\circ\text{C}$), we tested the association between the start and maximum temperature but did not find any significant correlation ($t = -0.737$, $p = 0.461$, Fig. S8a). Variation in surface temperature before the start of the heating experiment was significantly lower than the variation in the asymptotic maximum surface temperature at the end of the heating experiment (Fig. S8b).

To compare the temperature values measured with thermocouples and thermal imaging we ran a paired t-test on reference temperature. Temperature measured with the thermal camera was significantly higher than measured with the thermocouple (initial temperature T_0 : Diff = 0.334, $t = 16.438$, $p < 0.001$; heating rate k_2 : Diff = 0.0004, $t = 12.456$, $p < 0.001$; asymptotic maximum temperature T_∞ : Diff = 2.648, $t = 50.447$, $p < 0.001$). Moreover, the temperature difference for the reference measurements increased during the 10-minute heating process (Fig. S9). Therefore, we treated thermal camera and thermocouple measurements as separate variables in our analyses.

The curvature of the body of bird specimens could lead to differences in heating rates in the different body parts. To test whether the heating of different body parts varies regardless of color, we used the Fraser's Sunbird ($n = 10$) as a control specimen because all feathers are based on the same color producing mechanism and it shows the least variation in color considering all body parts (Fig. 2e). We first checked whether the brightness, which we assessed with the R package *pavo* [7], of the different body parts differed with an analysis of variance (ANOVA) and used a Tukey HSD test to compare the means (Fig. S10a). Secondly, we tested whether the heating rate k_2 and maximum temperature T_∞ differed in those

body parts that did not differ in brightness with an ANOVA (Fig. S10b, Fig. S10c). Since those values did not differ for breast 1, breast 2 and the belly (heating rate k_2 : $F = 0.874$, $p = 0.429$, maximum temperature T_∞ : $F = 0.745$, $p = 0.484$), we grouped those (hereafter referred to as “breast”) and ran our analyses on four groups: breast, throat, mantle and crown.

For the heating experiments, we chose species that highly differ in coloration and color composition across body parts. However, to test whether the choice of species could affect the analyses, we assessed the phylogenetic signal on mean brightness of each body part in male sunbirds using the R package `phytools` [8] and `caper` [9] based on the species-level avian phylogeny from the Bird Tree Project [10]. The phylogenetic signal in mean brightness of the male sunbirds used in this study was low for most body parts (upper breast, belly, mantle, throat) ($\lambda \leq 0.4$, Fig. S11), thus we did not account for phylogeny in these models. The phylogenetic signal in mean brightness of the lower breast and the crown however was high ($\lambda = 0.9$ and $\lambda = 0.7$), yet the linear model on maximum surface temperature and mean brightness showed similar results when accounting for phylogeny (Table S4).

Supplemental figures

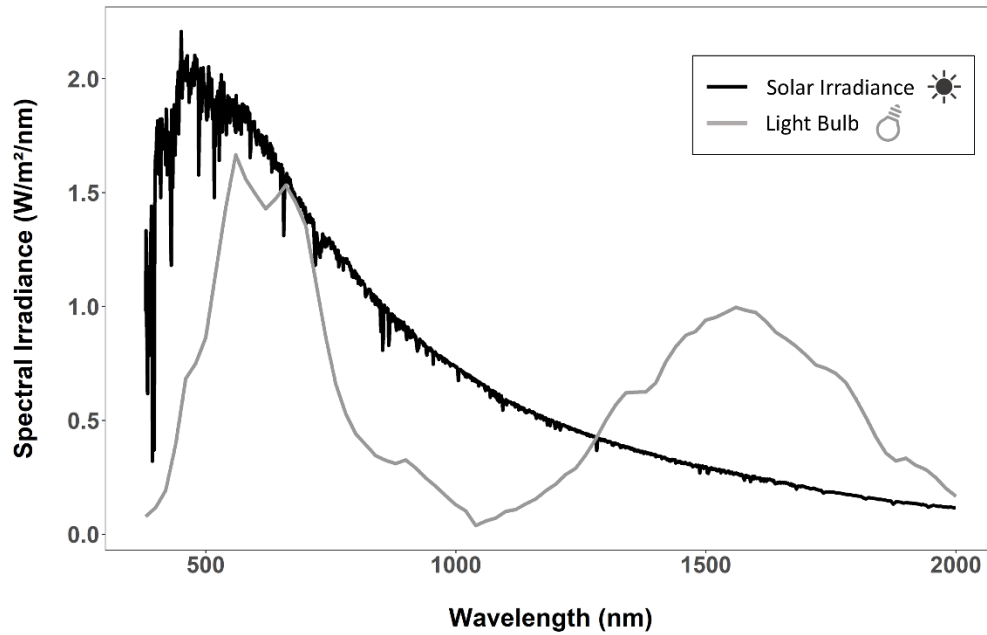
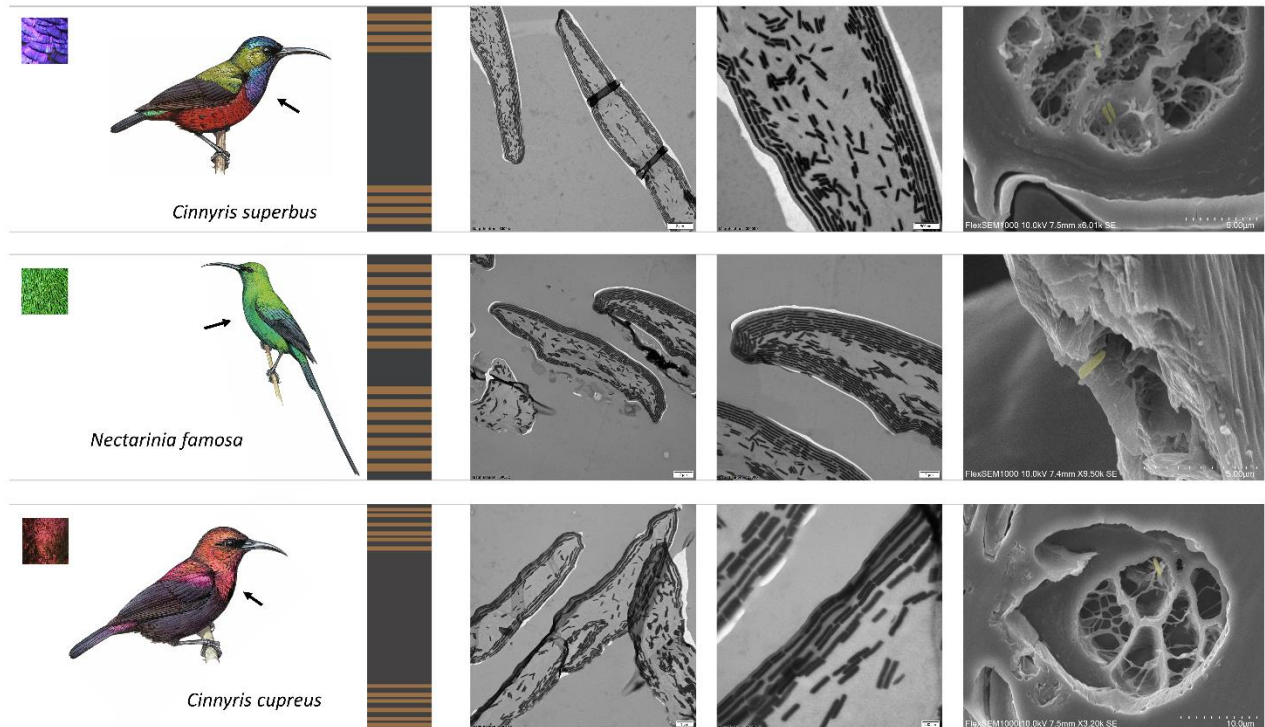


Fig. S1: Comparison of spectral irradiance of the sun by Gueymard [5] and the Philips NIR light bulb used for the heating experiments on museum specimens over the visible and near infrared spectrum. Solar irradiance (W/m²/nm) reflects the radiation reaching the earth's surface, while lamp irradiance was normalized for an intensity of 1000 W/m², the light intensity that reached the feather surface during the experiment. The spectral power distribution is provided in Table S2.



Color	Shape	Nr of layers	Height of melanosomes (nm)	Width of melanosomes (nm)	Length of melanosomes (nm)	Outer keratin layer (nm)
Purple	Platelets	4	90	316	1229	110
Green	Platelets	7	100	627	1569	130
Copper	Platelets	6	50	417	1910	40
Black	Rods	3	135	280	1450	75
Grey	Spheres	-	70	103	70	-
White	-	-	-	-	-	-

Fig. S2: Setup for idealized models of feather barbules based on transmission electron microscopy (TEM) and scanning electron microscopy (SEM) images. A selection of electron microscopy images is shown for the iridescent feather barbules (purple, green, copper). Melanosomes in the TEMs (first two photo columns) are black and in the SEM (right photo column) visualized in yellow. The table beneath provides information on size and shape of melanosomes, the number of melanosome layers as used in the model and the average width of the outer keratin layer.

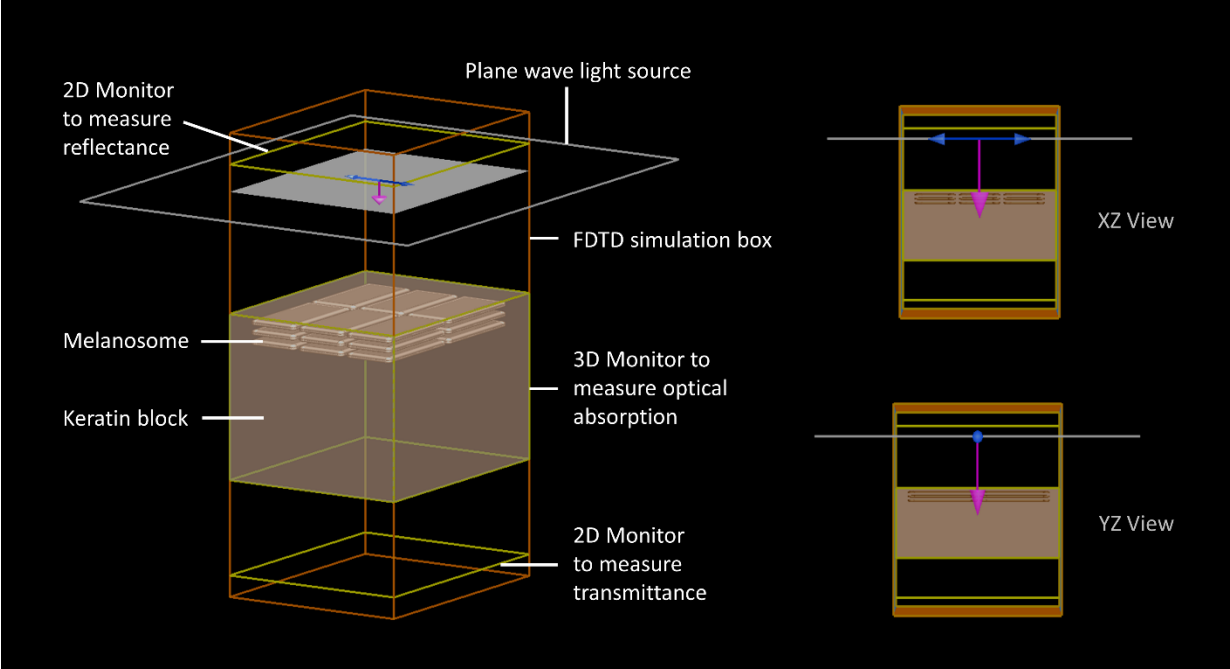


Fig. S3: Typical setup of a FDTD simulation box. Our models were set up as a keratin block (grey) with integrated melanosomes (brown) of different shapes and sizes. For the light source we used a plane wave at normal incidence injected in the downward direction.

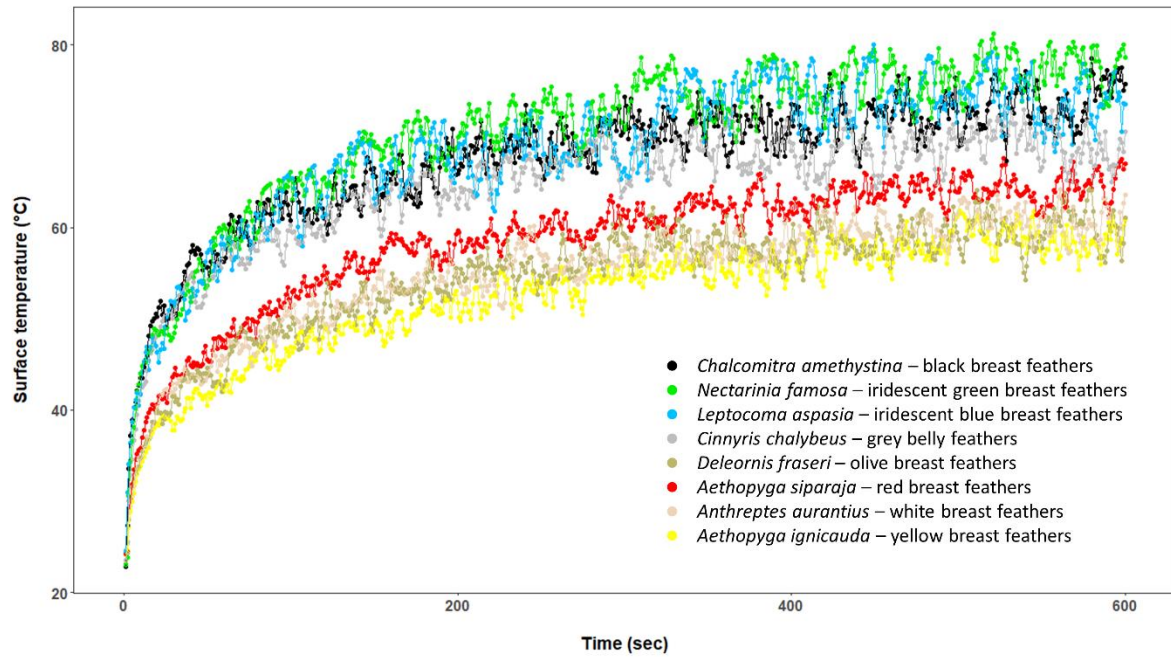


Fig. S4: Selection of heating curves of the feather surfaces as a function of time. We here show the raw data, i.e. the heating of different color patches in male sunbirds.

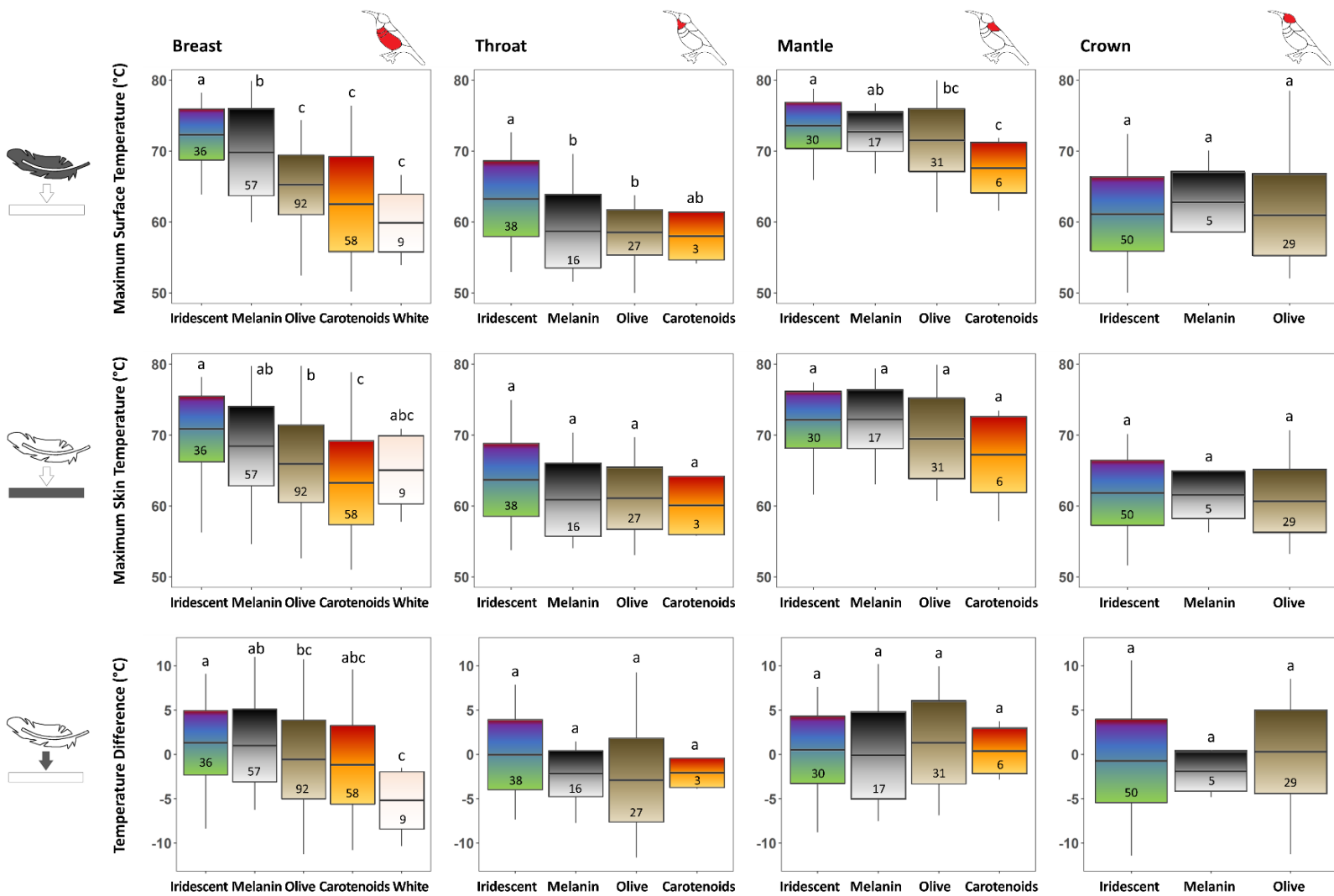


Fig. S5: Differences in mean maximum surface temperature, maximum skin temperature and the temperature difference between feather surface and skin (heat transfer), for different color producing mechanisms and body parts. We plotted the mean, standard variation and minimum and maximum value. We ran a Tukey HSD test to perform a multiple pairwise-comparison between the means of the groups. For categories that do not differ significantly ($p > 0.05$) the same letters are provided above the corresponding boxes. Numbers in the boxes represent the sample sizes.

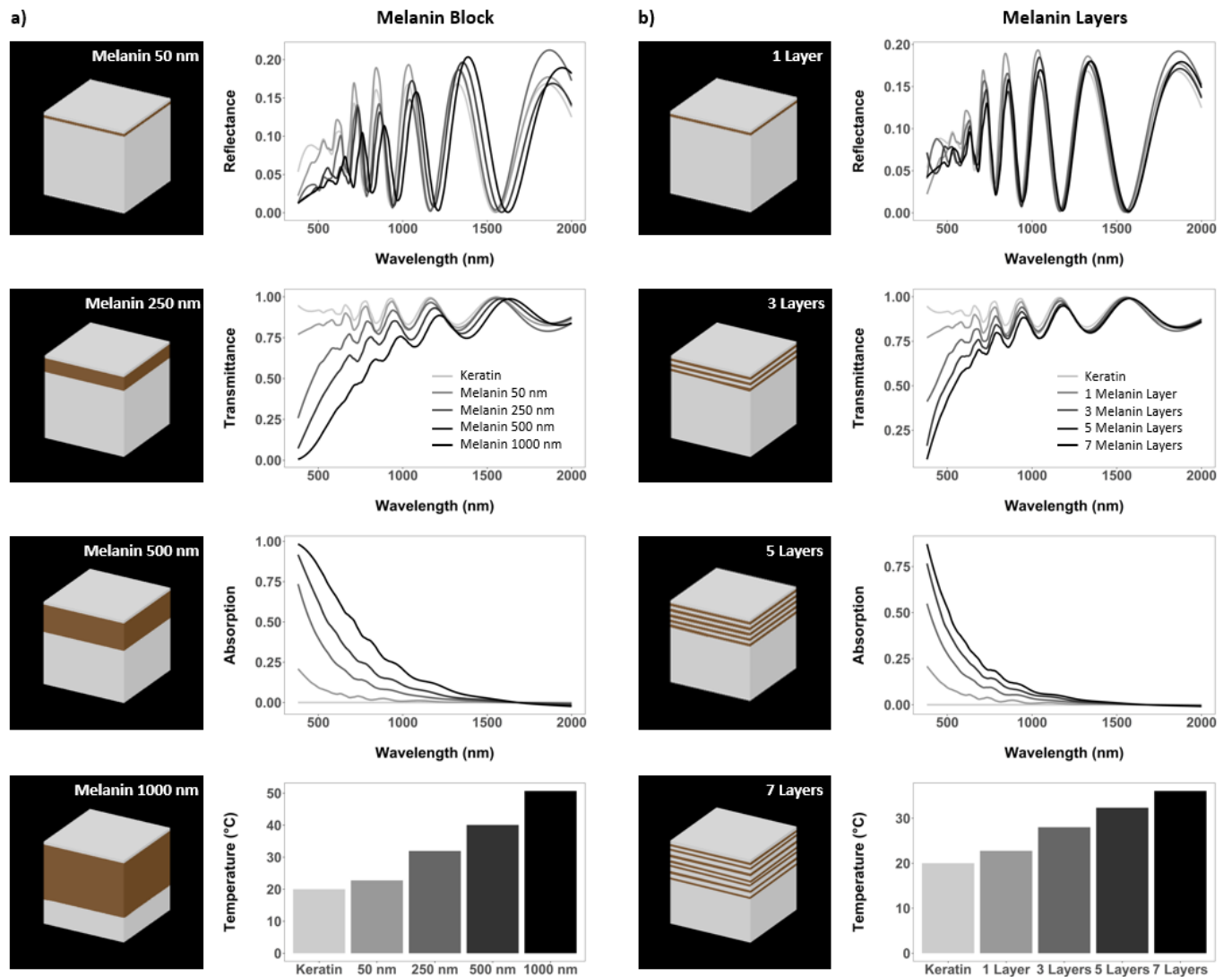


Fig. S6: Reflectance, transmittance, absorption and temperature were modeled for blocks of keratin (grey) with integrated melanin (brown). Blocks are half the height of an average feather barbule ($1.5 \mu\text{m}$) and differ from the feather model by lacking the mirrored layering of melanin and keratin. a) We increased the melanin content in the keratin block by varying the height of a single layer of melanin by 50, 250, 500, and 1000 nm. b) Melanin in feather barbules is generally arranged in layers, thus we tested for the effect of the melanin content in the feather barbules by adding 50 nm high melanin layers using 1, 3, 5 and 7 layers. For both model sets we found that with increasing melanin content transmittance decreases and absorption increases leading to a rise in temperature. Variation in reflectance with increasing melanin content mostly occurs within the visible spectrum.

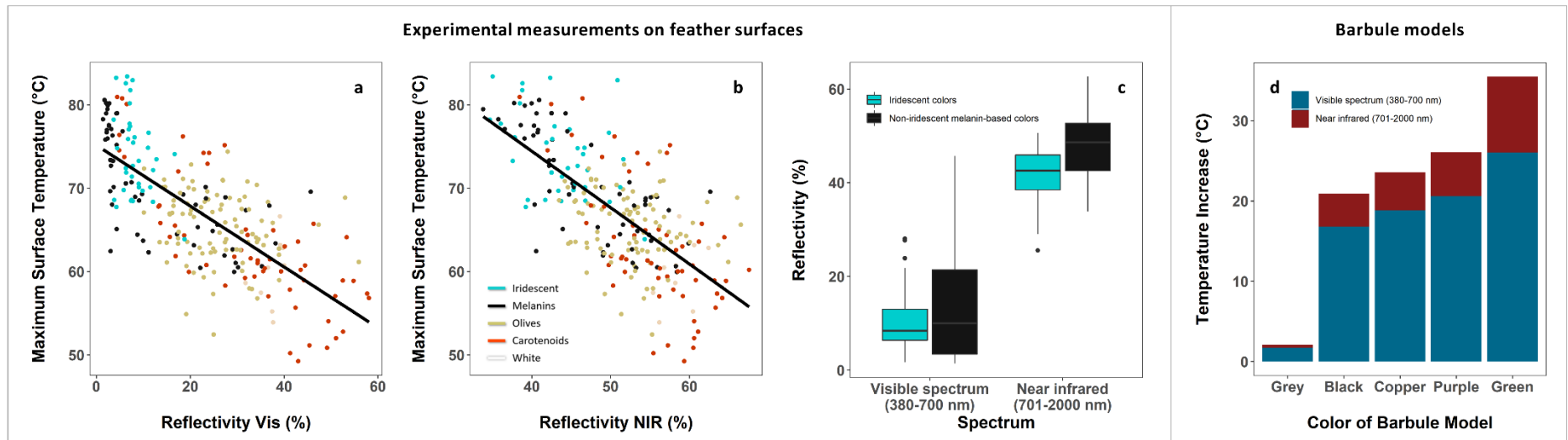


Fig. S7: In experimentally heated feather surfaces of sunbird museum specimens, asymptotic maximum temperature can be explained by both, a) reflectivity over the visible spectrum spanning 380 to 700 nm ($\beta = -0.37 \pm 0.02$, $p < 0.001$, $R^2 = 0.53$) and b) reflectivity over the near-infrared spanning 701 to 2000 nm ($\beta = -0.68 \pm 0.05$, $p < 0.001$, $R^2 = 0.47$). However, reflectivity of melanin-based iridescent and non-iridescent feathers differed slightly more in the near-infrared (Vis: $F_{1,91} = 4.79$, $p < 0.032$; NIR: $F_{1,91} = 6.61$, $p < 0.012$) (c). In modeled feather barbules (d), temperature increase can be explained to a large extent by a greater light absorption within the visible spectrum (380-700 nm) for all melanin-based colors, i.e., non-iridescent grey and black as well as iridescent copper, purple and green.

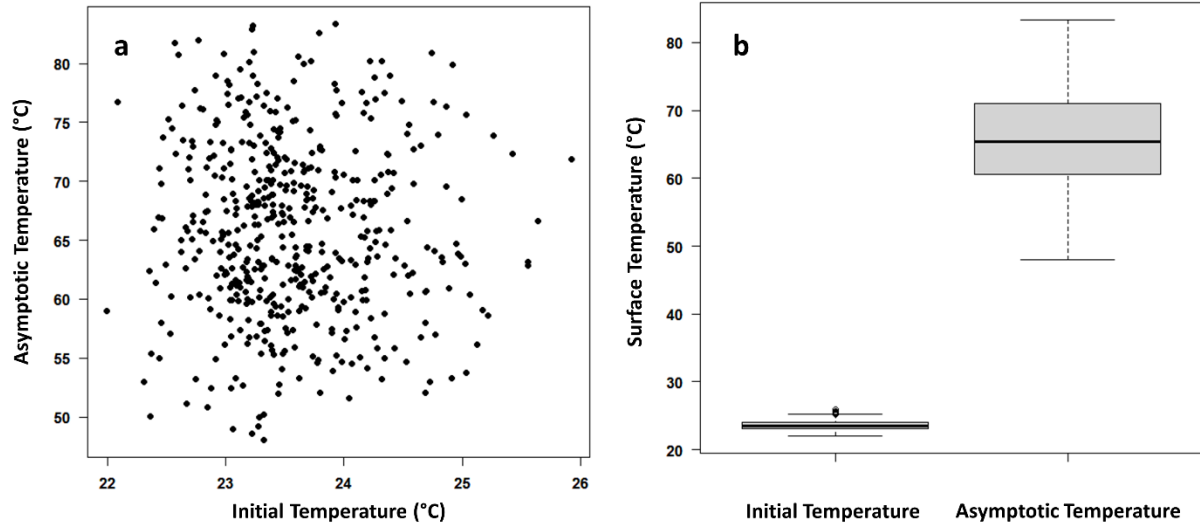


Fig. S8: a) The initial surface temperature T_0 (mean = $23.58 \pm 0.029^\circ\text{C}$) does not affect asymptotic maximum surface temperature T_∞ ($t = -0.737$, $p = 0.461$). b) Variation in surface temperature before the start of the heating experiment was significantly lower than the variation in the asymptotic maximum surface temperature at the end of the heating experiment.

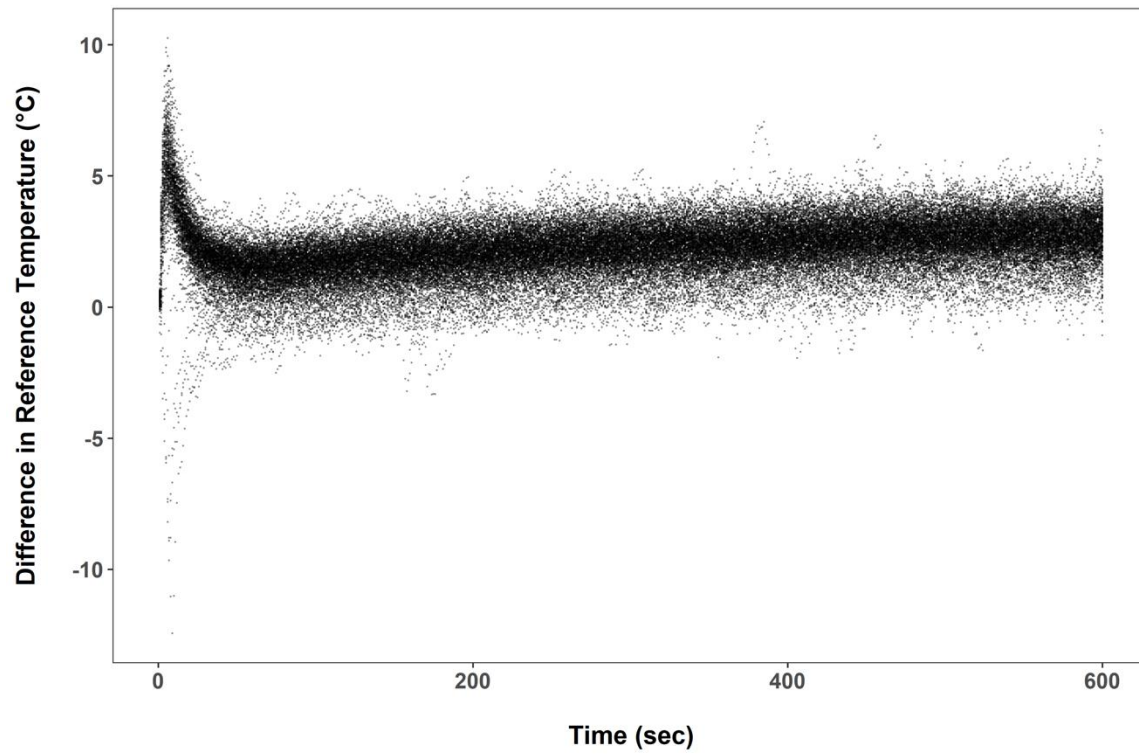


Fig. S9: Temperature difference between thermocouple and thermal camera measurement for the duration of the heating experiment.

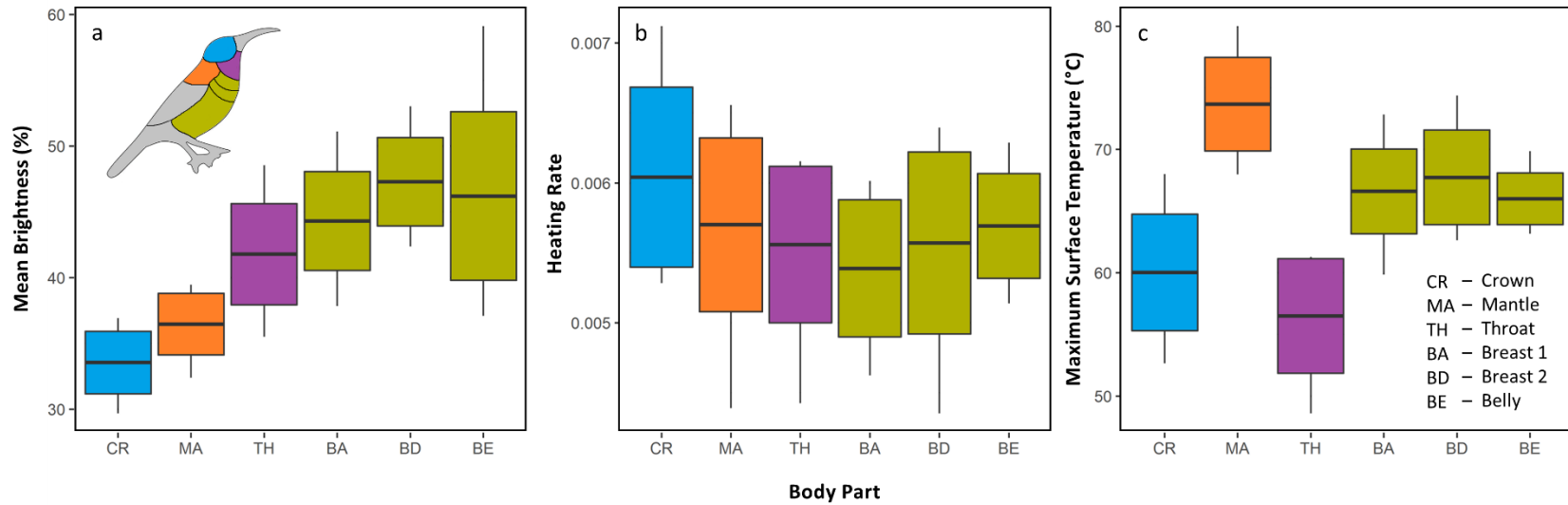


Fig. S10: a) Differences in mean brightness in all body parts of the control group (Fraser's sunbirds, $n = 10$). b) Differences in heating rate k and c) in asymptotic maximum temperature T_{∞} . Since brightness, heating rate and T_{∞} did not differ for breast 1, breast 2 and the belly, we grouped those. We plotted the mean, standard variation and minimum and maximum value.

Phylogenetic Signal in Mean Brightness

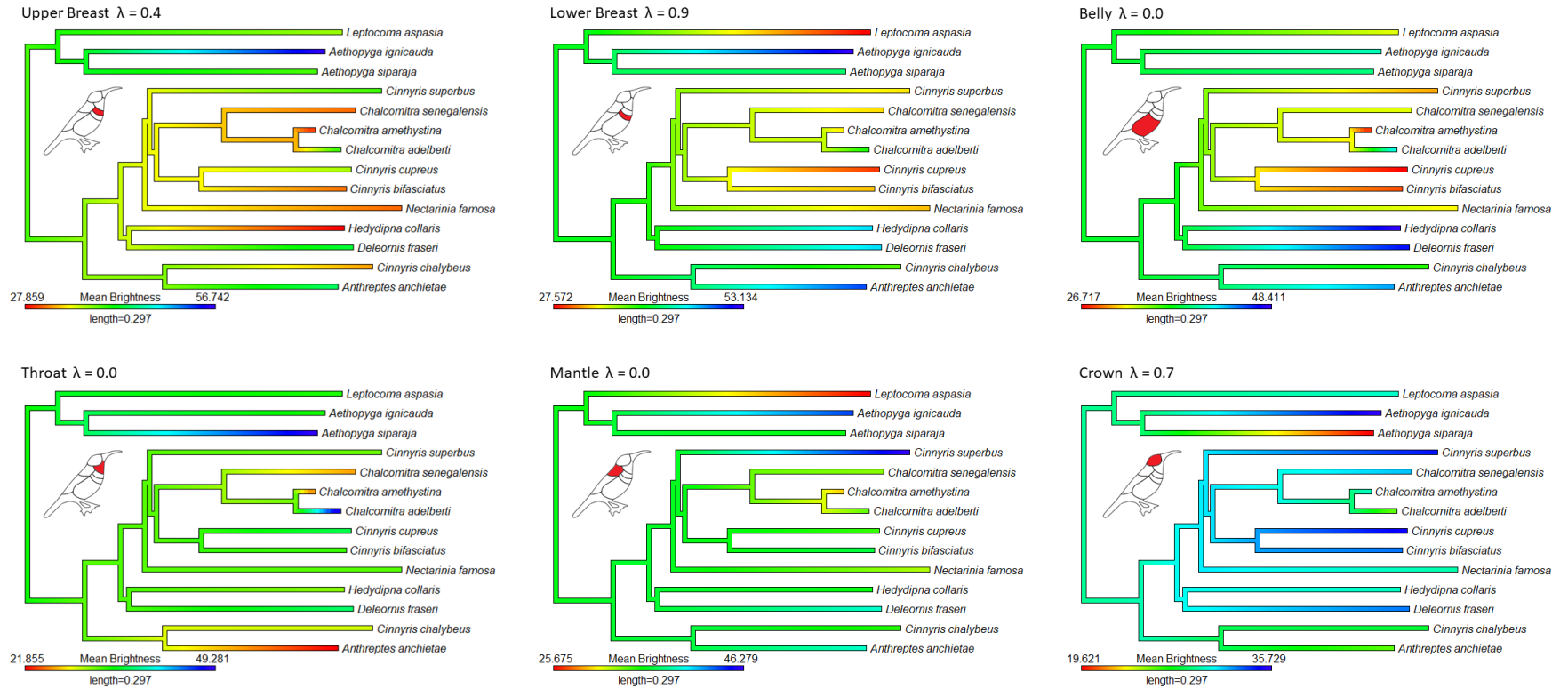


Fig. S11: Phylogenetic signal in mean brightness in male sunbirds for different body parts. We used the R package phytools [8] to assess the phylogenetic signal.

Supplemental tables

Table S1: Species list and numbers of males and females used for the heating experiments.

Species	males	females	Total
<i>Aethopyga ignicauda</i>	3	2	5
<i>Aethopyga siparaja</i>	3	2	5
<i>Anthreptes anchietae</i>	3	2	5
<i>Anthreptes aurantius</i>	3	3	6
<i>Chalcomitra adelberti</i>	3	2	5
<i>Chalcomitra amethystina</i>	3	3	6
<i>Chalcomitra senegalensis</i>	3	2	5
<i>Cinnyris bifasciatus</i>	3	2	5
<i>Cinnyris chalybeus</i>	3	2	5
<i>Cinnyris cupreus</i>	3	3	6
<i>Cinnyris superbus</i>	3	2	5
<i>Deleornis fraseri</i>	5	5	10
<i>Hedydipna collaris</i>	3	3	6
<i>Leptocoma aspasia</i>	3	2	5
<i>Nectarinia famosa</i>	3	2	5

Table S2: Spectral power distribution of solar light compared to the heat lamp used in the experiments.

Range	Solar Light (W/m²) (total is 1196 W/m²)	Lamp (normalized to 1000 W/m²)
380-800 nm	685	428
800-1300 nm	345	117
1300-2000 nm	166	456
Percentage of power between 800-2000 nm	42.7 %	57.2 %

Table S3: Particle dimensions of model set to explore the effects of structural arrangement and shape of melanosomes on photothermal absorption (see Figure 10).

Melanosome Shape	Nr. of Particles	Radius X (nm)	Radius Y (nm)	Radius Z (nm)	
Sphere	75	50	50	50	
Ellipsoid	45	100	41.7	50	
		Radius (nm)	Roundness of the ends (nm)	Length (nm)	
Rod	30	140.2	67.2	657	
		X span (nm)	Y span (nm)	Z span (nm)	Radius of rounded edges (nm)
Platelet	18	300	600	90	30

Table S4: Linking maximum surface temperature to mean brightness shows similar results when correcting for the phylogenetic signal in brightness of lower breast and crown using PGLS analyses with the R package caper [9].

Method	Estimate	Std Error	p-value	R ²
Lower Breast				
Linear Model	-0.85	0.15	<0.001	0.7
PGLS	-0.88	0.16	<0.001	0.7
Crown				
Linear Model	0.32	0.30	0.30	0.01
PGLS	0.27	0.31	0.40	-0.02

References

- [1] Walsberg GE, Campbell GS, King JR. 1978 Animal coat color and radiative heat gain: a re-evaluation. *Journal of Comparative Physiology B: Biochemical, Systemic, and Environmental Physiology* **126**, 211-222. (<https://doi.org/10.1007/BF00688930>).
- [2] D'Alba L, Saranathan V, Clarke JA, Vinther JA, Prum RO, Shawkey MD. 2011 Colour-producing β -keratin nanofibres in blue penguin (*Eudyptula minor*) feathers. *Biology letters* **7**, 543-546. (<https://doi.org/10.1098/rsbl.2010.1163>)
- [3] Schneider CA, Rasband WS, Eliceiri KW. 2012 NIH Image to ImageJ: 25 years of image analysis. *Nature methods* **9**, 671-675. (<https://doi.org/10.1038/nmeth.2089>)
- [4] Stavenga DG, Leertouwer HL, Osorio DC, Wilts BD. 2015 High refractive index of melanin in shiny occipital feathers of a bird of paradise. *Light: Science & Applications* **4**, e243-e243. (<https://doi.org/10.1038/lsa.2015.16>)
- [5] Gueymard CA. 2004 The sun's total and spectral irradiance for solar energy applications and solar radiation models. *Solar energy* **76**, 423-453. (<https://doi.org/10.1016/j.solener.2003.08.039>)
- [6] Trapletti A, Hornik K. 2020 tseries: Time series analysis and computational finance. *R package version 0.10-48*.
- [7] Maia R, Eliason CM, Bitton PP, Doucet SM, Shawkey MD. 2013 pavo: an R package for the analysis, visualization and organization of spectral data. *Methods in Ecology and Evolution* **4**, 906-913.
- [8] Revell LJ. 2012 phytools: an R package for phylogenetic comparative biology (and other things). *Methods in ecology and evolution* **3**, 217-223.
- [9] Orme D, Freckleton R, Thomas G, Petzoldt T, Fritz S, Isaac N, Pearse W. 2012 Caper: comparative analyses of phylogenetics and evolution in R. *R package version 0.5 2*, 458.
- [10] Jetz W, Thomas GH, Joy JB, Hartmann K, Mooers AO. 2012 The global diversity of birds in space and time. *Nature* **491**, 444-448.